Understanding the design of warning signals: a predator's view

Olivier Pennacchio (op5@st-andrews.ac.uk)
University of St Andrews
Christina Halpin
Newcastle University
Innes C. Cuthill
University of Bristol
P. George Lovell
Abertay University
Matthew Wheelwright
Newcastle University
John Skelhorn
Newcastle University https://orcid.org/0000-0002-8385-4831
Candy Rowe
Newcastle University
Julie M. Harris
University of St Andrews https://orcid.org/0000-0002-3497-4503

Article

Keywords: Aposematism, animal pattern, prey defence, receiver psychology, sensory exploitation, natural images, Lepidoptera, Gallus gallus domesticus, camouflage, predation

Posted Date: August 13th, 2021

DOI: https://doi.org/10.21203/rs.3.rs-777244/v1

Abstract

Animal warning signals show remarkable diversity, yet subjectively appear to share visual features that make defended prey stand out and look different from more cryptic palatable species. Here we develop and apply a computational model that emulates avian visual processing of pattern and colour to Lepidopteran wing patterns to show that warning signals have specific neural signatures that set them apart not only from the patterns of undefended species but also from natural scenes. For the first time, we offer an objective and quantitative neural-level definition of warning signals based on how the pattern generates neural activity in the brain of the receiver. This opens new perspectives for understanding and testing how warning signals function and evolve, and, more generally, how sensory systems constrain general principles for signal design.

Introduction

Aposematic prey have striking colour patterns that warn potential predators that they are unpleasant or unprofitable to eat [1–5]. Despite their diversity in nature [6], some common visual characteristics, such as being yellow or red, or having 'high contrast internal boundaries' or 'repetitive elements', are thought to be the key features that enhance learned or unlearned aversions in predators [2,4,7,8]. However, studies do not consistently find that these specific visual characteristics are particularly effective at deterring predators [9–14], and any underlying general principles of warning signal design have yet to be identified and specifically quantified. Therefore, although aposematism has long been a textbook example of adaptation and a key testbed for evolutionary theory [4,8,15], we still don't know what makes warning signals effective.

In this paper, we take a radically different approach, testing the hypothesis that it is what the signals do to the brains of predators that is the unifying design principle. In recent years, methods from visual neuroscience have been successfully applied to camouflage patterns to understand how they reduce the chances that prey stimulate neurons involved in predators' visual detection systems [16–19]. Here, we significantly expand this approach, by developing a novel objective and quantitative framework based not only on the responses of classes of neurons, but on how the response of a whole visual network in predators may underlie the design of these signals. We make the strong prediction that the warning signals of aposematic prey will have been selected to produce specific neural signatures in the visual processing systems of their predators, that are different from neural responses to both natural scenes and the patterns of more palatable species. We propose that this neural activity defines the distinctiveness and conspicuousness that facilitate predator aversion. Our results indicate that there is a general principle of warning signal design that is shared by species that, superficially, might look very different from one another. Furthermore, our approach provides an objective measure of colour patterns that can underpin a wide range of future studies in animal coloration.

Results

A database of lepidopteran patterns

Whilst aposematism is taxonomically widespread, we focussed on how the colour patterns of Lepidoptera stimulate the visual systems of birds. This is a well-established model system for the study of defensive strategies, particularly aposematism and crypsis [20–22], and where the visual system of the predator is also relatively well understood [23]. From an initial literature search (see Methods for details), we built a representative database of 125 species of Lepidoptera for our analysis (96 aposematic and 29 non-aposematic species). Samples of each species were located in museum collections, and their dorsal and ventral sides were photographed using a hyperspectral camera (Fig. 1a,b).

Computational modelling of visual processing in the avian brain

Initially, we applied a model to emulate bird retinal vision, based on what we know about their photoreceptors. We used the best characterised model of avian vision, that of the chicken (*Gallus gallus domesticus*) [23]. Since colour and luminance are processed in distinct pathways, we separately estimated the response to the patterns of double cones, thought to underlie luminance perception in birds[23,24] (Fig. 1c); and responses using the four classes of simple cone photoreceptors respectively sensitive to ultraviolet (U), short (S), medium (M) and long (L) wavelength, which underlie colour perception[23] (Fig. 1f).

To investigate how variation in luminance is processed by the avian visual system, we built a model based on the neurobiological architecture likely to underlie luminance perception in birds. The luminance model consisted of units that encode luminance edges at specific topographical locations, for different orientations and spatial scales (coarse to fine). Our model was based on units found in the early visual system of mammals[25,26], but these are also thought to be analogous to neurons found in the avian visual system[27–29]. The response of each unit was then modulated by the responses of surrounding units following a standard centre-surround operation called 'divisive normalization', which is found extensively across sensory systems and increases the sensitivity to salient features [30,31] (Fig. 1c). To explore the variation in colour, we converted the responses of the simple cones into opponent channel information by considering the L-M ('red-green'), (L + M)-S ('yellow-blue'), and U-S ('ultraviolet-blue') channels, which are assumed to be at the basis of colour perception in birds[23]. We specifically selected the L-M channel for our colour analysis, as variation across the L-M and the (L + M)-S channels was highly correlated for the samples in our database and the response of the U-S channel was similar for the patterns of aposematic and non-aposematic prey (see Supplementary Result 1) (Fig. 1f). After this first stage of modelling, each hyperspectral photograph could be represented by two vectors of population activities (capturing activity at each location, orientation and spatial frequency) that capture how luminance and colour are neurobiologically encoded at the early stages of the avian visual system (Fig. 1d,g).

We then used our model of sensory encoding to test for differences between the colour patterns of aposematic and non-aposematic prey. We defined three summary statistics to characterise brain activity,

which we refer to as a 'neural signature' (for full range of statistics considered, see Supplementary Result 1). For luminance, we computed the 'luminance energy' of the patterns using the standard deviation of the luminance population activity, a metric that is a robust predictor of brain activity[32,33]. We also measured 'isotropy departure', defined as how the distribution of signal across orientations differ from that typically found in natural scenes. This metric was chosen because orientation is known to be important in scene perception and in object categorization[34,35] (Fig. 1e). For colour, we computed the 'colour energy', defined as the standard deviation of the L-M channel, akin to the computation of 'luminance energy' (Fig. 1h)[36]. These analyses delivered three numbers for each pattern, forming a neural signature that can be plotted in a 3-dimensional 'pattern space'[16] (Fig. 1i).

Aposematic species have patterns with distinctive neural signatures in the avian brain

Our next step was to test our prediction that the neural signatures of our aposematic and non-aposematic species differ.

(i) *Luminance*. The patterns of aposematic prey had more luminance energy (Fig. 2a, top-left panel; logistic regression, see Methods: $\chi^2 = 49.32$, df = 1, $p = 2.18 \times 10^{-12}$, ΔAIC = 90.1–137.4 = -47.3) and higher isotropy departure (Fig. 2a, middle panel, $\chi^2 = 50.28$, df = 1, $p = 1.33 \times 10^{-12}$, ΔAIC = 89.1–137.4 = -48.3) than non-aposematic prey. Although these two summary statistics were correlated (Spearman-rank r = 0.59, 95% confidence interval [0.47,0.70]), the predictive power of a model including both luminance energy and isotropy departure (Fig. 2a, right panel) was better than that of a model including luminance energy only ($\chi^2 = 15.47$, df = 1, $p = 8.36 \times 10^{-5}$, ΔAIC = 76.6–90.1 = -13.5), or including isotropy departure only ($\chi^2 = 14.52$, df = 1, $p = 1.39 \times 10^{-4}$, ΔAIC = 76.6–88.9 = -12.3). Plotted in a 2-dimensional pattern space, aposematic and non-aposematic species therefore tended to occupy different regions (Fig. 2b).

To explore the role of phylogeny, we repeated these comparisons in the five families in our dataset that had both aposematic and non-aposematic species (Erebidae, Geometridae, Nymphalidae, Pieridae and Pyralidae). We used a bootstrapping procedure to draw pairs randomly (with replacement) to repeatedly resample the maximum number of possible pairs in these families, namely 26, and estimated the luminance summary statistics for the two categories of patterns (see Supplementary Result 3). Consistent with our overall findings, we found that both luminance energy and isotropy departure were higher for aposematic than non-aposematic pair members in the five families (bootstrap procedure, all $p < 10^{-6}$, see Supplementary Result 3, with only luminance energy higher in Pieridae).

(ii) *Colour*. Colour energy was significantly higher in aposematic than non-aposematic prey (Fig. 3a, left panel, $\chi^2 = 33.97$, df = 1, $p = 5.59 \times 10^{-9}$, ΔAIC = 105.4–137.4 = -40.0). Similarly to luminance, this result was found consistently when considering pairs of species made of an aposematic species and a randomly associated non-aposematic species in the same family ($p < 10^{-6}$ in the five families with both aposematic and non-aposematic species, Supplementary Result 3).

(iii) Combination of luminance and colour. Combining colour and luminance better discriminates between aposematic and non-aposematic patterns than either dimension alone. The predictive power of a model combining colour energy with the two luminance summary statistics (Fig. 3b) was higher than that of a simpler model including only the two luminance summary statistics (χ^2 = 5.66, df = 1, p = 0.0174, ΔAIC = 73.0–76.4 = -3.4) or the colour summary statistics only (χ^2 = 36.48, df = 1, p = 1.20 x 10^{-8}, ΔAIC = 73–105.5 = -32.5). We also visualised luminance energy, isotropy departure and colour energy in a 3-dimensional pattern space (Fig. 3c). The space can be separated into two regions, with aposematic patterns typically associated with higher values for the three summary statistics compared to non-aposematic patterns. The separation classified correctly 87.2% of the species.

Aposematic species have patterns that stand out in typical natural scenes

Aposematic signals are thought to have been selected to not only enhance predators' abilities to discriminate between palatable and defended prey, but to also increase prey conspicuousness in natural environments and enhance predator avoidance [8]. Specifically, we predicted that since visual detection is easier for objects with higher luminance or colour energy [32,36]; aposematic prey should have higher values for these metrics compared to natural scenes, with non-aposematic prey more likely to match natural scenes to enhance crypsis.

To test these predictions, we first presented patches of natural scenes to our model to extract their luminance and colour neural signatures. We then compared the differences in frequency distributions of our three summary statistics between natural backgrounds and those for aposematic and non-aposematic prey (Fig. 4). In support of our predictions, we found that aposematic patterns had frequency distributions with higher values compared to those of natural backgrounds, for all three summary statistics (luminance energy, $\bar{z} = 0.55$, Fig. 4a; isotropy departure, $\bar{z} = 1.43$, Fig. 4b; see Supplementary Result 4; colour energy, $\bar{z} = 1.72$, Fig. 4c). In contrast, the frequency distributions for non-aposematic prey were a much closer match to those of natural scenes, and even slightly lower in the case of luminance energy (luminance energy, $\bar{z} = -0.67$, Fig. 4a; isotropy departure, $\bar{z} = 0.04$, Fig. 4b; colour energy, $\bar{z} = 0.21$, Fig. 4c). This suggests that these aposematic patterns do not simply have colours and patterns that are different from those found in natural scenes but have been selected to deliver a stronger neural signature, and be more conspicuous in the natural world.

Discussion

By applying techniques from visual neuroscience to the study of aposematism, we show that Lepidopteran warning signals produce characteristic neural signatures in avian predators' brains. These warning signals share common design principles that exploit the ways in which predators' visual systems process complex natural scenes to make aposematic prey "stand out", both in the environment and with

respect to the patterns of undefended species. Our quantitative framework represents a step change in the study of aposematism by demonstrating that warning signals are best defined not by specific pattern elements [2,4,8], but rather by how the entire pattern generates neural activity. Crucially, this novel approach changes the way we view aposematism, and has important implications for how we measure and study warning signals. It could also be applied to a number of signalling systems, promoting a wide-ranging reassessment of the way we view signal evolution.

Our findings have clear implications for the way in which we conceptualize aposematism. They suggest that the ultimate function of warning signals is not to exploit some unspecified biases in predator learning and memory towards particular colours or pattern elements [8,12,37] (e.g., being red or having stripes), but instead to elicit strong and distinct neural signals in predators' brains. Such a shift in thinking about what warning signals are ultimately designed to do offers a number of insights. Firstly, it may help explain why warning signals are easier to learn and remember. Special cognitive effects may rely on what the brain does in response to patterns, not on the specifics of the pattern. Secondly, it helps us to better understand warning signal diversity and predict signal efficacy. As we have shown, there are many ways to produce a strong neural signature, meaning that a range of patterns that look very different may affect predators in very similar ways (see Fig. 3). Being able to quantify the neural activity elicited by prey patterns means we can now more precisely predict the relative strength of different warning signals. This will allow us to better identify species with patterns that fall outside what we consider the norm, and challenge the assumption that warning signals without typical features are somehow 'weak' and less effective [38,39].

Having a colour pattern space where dimensions correlate with receiver's perception is the gold standard for understanding the evolution of animal coloration [16], and our approach provides exactly this. It allows us to measure patterns in a more biologically relevant way, and predict the strength of a warning signal based on its position in our pattern space. Our work has compared animal patterns against a wide range of generic signalling environments, so is immediately applicable for aposematic species that use a range of visually distinct habitats [40,41]. It is possible that the separation in pattern space between animal pattern and habitat might be even stronger if the specific signalling background was known. The computational tools we have developed can also be used to significantly enhance empirical approaches to assessing what features make aposematic colour patterns effective. Previous work in this area has predominantly manipulated those specific pattern features thought to be important, such as being red or striped, and then measuring the effects changes have on prey survival (e.g., [9,13,42–44]). However, these kinds of manipulations automatically alter other aspects of the whole pattern, explaining why such studies are often difficult to interpret [44,45]. In contrast, our approach allows us to not only know how manipulations alter how the whole signal is perceived by predators, but also to generate completely novel stimuli that sit in different areas of pattern space and vary in the degree to which they share features with aposematic patterns from a predator's perspective.

Our approach is based on well-known components of visual systems that are likely to be conserved across a range of species [46,47], meaning that it could potentially be used to study the patterns of animals across different contexts with a wide variety of receivers. Whilst our model could be refined as we learn more about avian brains, especially the machinery of avian colour vision, the key point is that it enables a paradigm shift in the study of visual communication. In short, visual communication needs to be understood from the perspective of how signals stimulate receivers' brains [7,48–50], and particularly, how visual systems are designed to code information. Two recent studies have considered male sexual signals from a similar perspective, and suggest that they could be designed to enhance female preferences by being processed more efficiently [51,52]. Our findings show that knowledge of signal processing is also key to understanding a very different class of signal. However, crucially the mechanism through which this occurs is in stark contrast to previous studies: signal efficacy in increased by being more costly to process [53–55] rather than more efficient [50–52]. Consequently, our findings have wide-ranging implications for the study of signal design by raising the intriguing possibility signals intended to attract receivers are selected to enhance processing efficiency, and those intended to deter or repel receivers are selected to inhibit it. Understanding how different classes of animal signals are designed to elicit quantifiably different neural and behavioural responses in will be a fruitful area for future study.

Methods

Building a database of Lepidoptera patterns. We first searched Google Scholar from 1980 onwards using the term "aposem*". From the studies returned in this search, we identified aposematic Lepidopteran species, and selected them for our study where evidence was consistent with them being defended (for example, being rejected by predators, or larvae feeding on toxic host plants). We then searched for 'palatable' species from the same families for a representative sample of palatable non-aposematic species (any Batesian mimics of aposematic species were excluded). Again, we checked the literature for evidence of palatability for each species used. In total, we identified 96 aposematic (AP) species, and 29 palatable, non-aposematic (non-AP) species from the same families which could be sourced from museum collections. We collected hyperspectral images using museum specimens from the Natural History Museum (BMNH), London, UK, the Manchester Museum (MMUE), Manchester, UK, and the American National Museum (AMNH), New York, USA. In total, we photographed the dorsal and ventral sides of 331 specimens (AP, N = 244, average number of specimens per species 5.1, std 2.9; non-AP, N = 87, average 6, std 2.8) from the selected species, giving a total of 676 hyperspectral images. Two specimens were removed from the analysis because no scan of their ventral side had been recorded. See Table S1 and Table S2 for a full list of respectively all the species and specimens that were imaged, and online Supplementary Information for a description of these tables.

Hyperspectral image acquisition. *Imaging system*. To acquire the database of Lepidoptera we used a hyperspectral imaging system built around an ultraviolet hyperspectral imaging camera (Resonon Pika NUV (Resonon Inc., MT USA) covering the 350 nm – 800 nm spectral range, with a spectral resolution of 1

nm.) The camera was fitted with a near ultraviolet 17 mm focal length objective lens. To maximize the homogeneity of the light field, the specimens were illuminated by four blue enhanced halogen lamps (SoLux, 35W, 12V-MR16 GU5.3 4700K) placed 22 cm apart on a squared fixture light and oriented vertically toward the horizontal scanning plane. *Spatial calibration*. The hyperspectral camera acquires data one line at a time. It then reconstructs a two-dimensional image by joining up the consecutive lines collected by translating the camera along the object in the direction perpendicular to that of the camera's imaging line. The resulting hyperspectral images are three-dimensional tables of size px_slit x px_image x N_λ, where px_slit is the number of pixels in the imaging line, px_image is the number of lines scanned along the direction of translation, and N_λ= 451 is the number of spectral bands considered. We carefully set the scanning speed to ensure that relative distances in the real scene were preserved in the scanned image for all directions in the image plane (Supplementary Method 1). *Spectral calibration*. Once the illumination had stabilized, 20 minutes after switching the lights on, the dark current was measured by blocking the objective lens with a cap. We then placed a reference piece of pure polytetrafluorethylene (Berghof optical PTFE 98%, Berghof Fluoroplastic Technology GmbH, Eningen, Germany) in the scanning plane. This material has a diffuse reflection, and a flat reflectance spectrum in the range of frequencies we considered, 350 nm – 800 nm (minimum reflectance of 0.978 at 350 nm, average of 0.991 ± 0.0053 std over the range of frequencies). The measurement of the reference piece was used to calibrate the imaging system by correcting for the effects of illumination and obtaining the absolute reflectance of the specimen, scaled between 0 (reflectance 0) and 10^5 (reflectance 1), using a standard procedure provided by the software (SpectrononPro 2.101, Resonon Inc., MT, USA). The spectral calibration was repeated periodically during the scanning sessions. *Specimen setting*. Each tethered specimen of Lepidoptera was placed on a background made of matte and diffuse black flocked paper (Thorlabs, Inc., Newton, NJ, USA) with its height adjusted so that the wing plane coincided with the scanning plane. All the specimens were scanned with the same distance to the objective lens (237 mm) to ensure that the relationship between pixel size in the hyperspectral images and the specimen's real size was the same for the whole database. The database consists of 662 hyperspectral images and is available at https://arts.st-andrews.ac.uk/lepidoptera/.

Modelling the avian visual system. We developed a model to simulate the effect of Lepidoptera patterns on avian perception. The model emulates the neural response of the avian early visual system to any pattern, with luminance and colour treated separately to reflect the evidence that colour and luminance are processed in separate pathways in the avian visual system[23]. *Luminance*. Double cone photoreceptors are thought to be responsible for luminance processing in birds and underpin the first stage of edge, contour and texture perception[24,56,57]. The hyperspectral images were first converted into luminance using the spectral sensitivity of double cones in the chicken (*Gallus gallus domesticus*) retina, taking into account media absorption and oil droplet correction[58,59]. Luminance information was then processed by a population of model 'units' distributed topographically on a regular grid, emulating neurons tuned to respond to edge information at different spatial locations, orientations and spatial scales. The receptive fields of these units were modelled using Gabor functions[60]. Technically, the response of a unit is obtained by convolving the luminance image with the receptive fields of the unit[61].

To consider only information about pattern rather than contrast with the background, we discarded responses from the units whose receptive fields were not totally included within the area defined by the specimen body. For every location in each Lepidoptera image, these computations yielded the strength of response to luminance edges at a number of different spatial scales and orientations (Fig. 1c). For each image, this modelling gave a vector of values providing a biologically plausible neural representation of the first stages of luminance pattern perception in the avian brain (Fig. 1d). Supplementary Method 2 provides a complete technical description of the part of the model based on luminance. *Colour*. We converted the hyperspectral images into cone responses using the quantum catches of the ultraviolet (U), short (S), medium (M) and long (L) wavelength sensitive cones, using the spectral sensitivity of these receptors for chicken, corrected for media absorption and oil droplets[58,59], and the spectrum of a standard daylight illuminant (D65)[58,59,62] (Fig. 1f, left). To emulate colour processing, we followed the modelling of opponent chromatic signals described in[23] and focussed on the output of the 'red-green' channel, $L - M$ (Fig. 1f, right). We obtained a vector of values that represented how 'red-green' information in the pattern was encoded in the avian brain. See Supplementary Method 2 for a comprehensive description.

Extraction of pattern neural signatures. To determine a global 'neural signature' of a Lepidoptera pattern, we extracted summary statistics of the model encoding activity in response to the pattern, related to established correlates of pattern, texture and colour perception. We considered two statistics based on luminance information and one based on colour. (i) *Luminance energy*. The luminance energy for encoding a pattern was computed as the contrast energy of the model encoding activity in response to the pattern, in other words as the standard deviation of the vector of responses of the units in the model. Variation in contrast-energy is a robust predictor of stimulus visibility and strength of brain activity[32,33]. (ii) *Isotropy departure*. Our measure of distribution of orientations considered how the evenness of the distribution of edge orientations at each location on the patterns compares to the typical evenness found in natural images. Orientation distributions are important in scene perception and object categorization[34,35,54]. (iii) *Colour energy*. The colour energy for encoding a pattern was computed as the contrast energy of the $L - M$ opponent channel, i.e., as the standard deviation of the vector of responses to the pattern of the modelled 'red-green' units. This colour counterpart of luminance energy is a strong predictor of stimulus visibility[36]. Thus, our summary 'neural signature' provided three numbers per pattern. Lepidoptera in the database varied in size, with body area ranging from 1.15 to $90.10 cm^2$ (mean 14.09, standard deviation 10.43). Importantly, the three neural signatures considered allowed us to compare different patterns independently of their size as the signatures are scale-invariant: they do not depend on the size of the pattern. Full technical details on neural signatures are given in Supplementary Method 3.

Natural scenes. We computed the luminance neural signatures of natural images using 4096 randomly selected patches of size 512 x 512 pixels in the subset of van Hateren's database of calibrated natural images that do not contain man-made objects[63]. For the colour neural signature, we considered 1024 patches of size 512 x 512 in Foster and Nascimento's database of hyperspectral natural images,

discarding images with man-made objects[64]. While this database does not include the UV range, it includes the full range of frequencies used for computing the response of L and M cones, and therefore the colour signature.

Statistical analyses. We used logistic regressions to analyse the relationship between the categorical variable 'pattern category' (AP, non-AP) and the continuous variables luminance energy, isotropy departure and colour energy. Logistic models were fitted in R[65] using generalized linear models (function *glm*). Standard hypothesis testing was done using likelihood ratio tests against a χ^2 distribution whose degrees of freedom was the difference in degrees of freedom of the models. Models were also compared using the Akaike Information Criterion (function *AIC*). The logistic regressions were also used to predict the probability of a pattern's category (AP, non-AP) given the neural signatures of the pattern. The boundaries for the binary classification in the pattern spaces shown in Fig. 2 (2-dimensional, luminance) and Fig. 3 (3-dimensional, luminance-colour) correspond to a threshold probability p(aposematism) = 0.5.

To analyse how the energy, isotropy and colour statistics compared within Lepidoptera families, we used generalized linear mixed models fitted in R with the function *glmer* in the package lme4[66]. We compared models with and without the binary independent variable 'pattern category' with 'family' as a random factor.

As a measure of the difference between the patterns and the natural backgrounds they might be seen against, we used signed z-scores (how many SD's the mean of each distribution is away from that of the natural scene distribution). To compute this, we shifted and scaled the signature to have an axis in which the distribution for natural scenes was standardized (i.e., had a mean of 0 and a SD of 1) and next computed the mean of the transformed signature for AP and non-AP patterns. The distributions of neural signatures of AP, non-AP patterns and natural scenes (Fig. 4) are kernel distributions computed using Matlab's[67] function *ksdensity* with default parameters, i.e., using a normal kernel function.

Declarations

Acknowledgements

We would like to thank Diana Umeton and Grace Holmes for their help with data collection, Geoff Martin (BMNH) for access to specimens and logistical support, Courtney Richenbacher and David Grimaldi (AMNH), and Dmitri Logunov and Phil Rispin (MMUE) for providing us with specimens. This work was funded by BBSRC grants awarded to J.M.H. and O.P. (BB/N006569/1), C.R. and J.S (BB/N00602X/1), P.G.L (BB/N005945/1), and I.C.C. (BB/N007239/1).

Author contributions

Following CRediT taxonomy: Conceptualisation: OP/JH/CR/JS/IC; Data curation: OP/CH/CR/JH; Software: OP;

Formal Analysis: OP/JH/IC; Methodology: OP/CH/JH/CR/JS/IC/GL; Investigation: OP/CH/MW; Administration/supervision: JH/CR/JS; Visualisation: OP; Writing – original draft: OP/JH/JS/CR; Writing – review and editing: All; Funding: OP/JH/CR/JS/IC/GL

Competing interests

The authors declare no competing interests.

Additional information

Supplementary Information is available at <https://to be determined>.

Data and code availability

All the hyperspectral images are available at https://arts.st-andrews.ac.uk/lepidoptera/.The data, Matlab and R code that support the findings of this study are openly available at Dryad, Dataset, https://doi.org/10.5061/dryad.x3ffbg7kd. (Link for private access: https://datadryad.org/stash/share/r7UMw-SMbQe6brENF_lc-lohuNMhNLXMNPBAHfzK-lY.)

References

1. Wallace, A. R. Discussion, March 4th meeting. *Transactions of the Royal Entomological Society of London* **Series 3**, **volume 5**, lxxx-lxxxi (1867).
2. Poulton, E. B. *The Colours of Animals: their meaning and use especially considered in the case of Insects*. (New York: D. Appleton and Company, 1890).
3. Cott, H. B. *Adaptive Coloration in Animals*. (London: Methuen & Co. Ltd., 1940).
4. Mappes, J., Marples, N. & Endler, J. A. The complex business of survival by aposematism. *Trends Ecol. Evol.* **20**, 598–603, doi:10.1016/j.tree.2005.07.011 (2005).
5. Rowe, C. & Halpin, C. Why are warning displays multimodal? *Behavioral Ecology and Sociobiology* **67**, 1425–1439, doi:10.1007/s00265-013-1515-8 (2013).
6. Briolat, E. S. *et al.* Diversity in warning coloration: selective paradox or the norm? *Biological Reviews* **94**, 388–414, doi:10.1111/brv.12460 (2019).
7. Guilford, T. & Dawkins, M. S. Receiver psychology and the design of animal signals. *Trends Neurosci.* **16**, 430–436, doi:10.1016/0166-2236(93)90068-w (1993).
8. Stevens, M. & Ruxton, G. D. Linking the evolution and form of warning coloration in nature. *Proceedings of the Royal Society B-Biological Sciences* **279**, 417–426, doi:10.1098/rspb.2011.1932 (2012).
9. Lindstrom, L., Alatalo, R. V. & Mappes, J. Reactions of hand-reared and wild-caught predators toward warningly colored, gregarious, and conspicuous prey. *Behavioral Ecology* **10**, 317–322, doi:10.1093/beheco/10.3.317 (1999).

10. Rowe, C. & Guilford, T. Novelty effects in a multimodal warning signal. *Anim. Behav.* **57**, 341–346, doi:10.1006/anbe.1998.0974 (1999).
11. Roper, T. J. & Wistow, R. Aposematic coloration and avoidance learning in chicks. *Q. J. Exp. Psychol. Sect. B-Comp. Physiol. Psychol.* **38**, 141–149 (1986).
12. Aronsson, M. & Gamberale-Stille, G. Importance of internal pattern contrast and contrast against the background in aposematic signals. *Behavioral Ecology* **20**, 1356–1362, doi:10.1093/beheco/arp141 (2009).
13. Hauglund, K., Hagen, S. B. & Lampe, H. M. Responses of domestic chicks (Gallus gallus domesticus) to multimodal aposematic signals. *Behavioral Ecology* **17**, 392–398, doi:10.1093/beheco/arj038 (2006).
14. Exnerova, A. *et al.* Avoidance of aposematic prey in European tits (*Paridae*): learned or innate? *Behavioral Ecology* **18**, 148–156, doi:10.1093/beheco/arl061 (2007).
15. Cuthill, I. C. *et al.* The biology of color. *Science* **357**, 7, eaan0221, doi:10.1126/science.aan0221 (2017).
16. Stoddard, M. C. & Osorio, D. Animal coloration patterns: linking spatial vision to quantitative analysis. *American Naturalist* **193**, 164–186, doi:10.1086/701300 (2019).
17. Stevens, M. & Cuthill, I. C. Disruptive coloration, crypsis and edge detection in early visual processing. *Proceedings of the Royal Society B-Biological Sciences* **273**, 2141–2147, doi:10.1098/rspb.2006.3556 (2006).
18. Troscianko, J., Skelhorn, J. & Stevens, M. Quantifying camouflage: how to predict detectability from appearance. *BMC Evol. Biol.* **17**, 7, doi:10.1186/s12862-016-0854-2 (2017).
19. Pike, T. W. Quantifying camouflage and conspicuousness using visual salience. *Methods Ecol. Evol.* **9**, 1883–1895, doi:10.1111/2041-210x.13019 (2018).
20. Cuthill, I. C. *et al.* Disruptive coloration and background pattern matching. *Nature* **434**, 72–74, doi:10.1038/nature03312 (2005).
21. Kapan, D. D. Three-butterfly system provides a field test of mullerian mimicry. *Nature* **409**, 338–340, doi:10.1038/35053066 (2001).
22. Ronka, K. *et al.* Geographic mosaic of selection by avian predators on hindwing warning colour in a polymorphic aposematic moth. *Ecology Letters* **23**, 1654–1663, doi:10.1111/ele.13597 (2020).
23. Osorio, D., Vorobyev, M. & Jones, C. D. Colour vision of domestic chicks. *J. Exp. Biol.* **202**, 2951–2959 (1999).
24. Bhagavatula, P., Claudianos, C., Ibbotson, M. & Srinivasan, M. Edge Detection in Landing Budgerigars (*Melopsittacus undulatus*). *PLoS One* **4**, 10, doi:10.1371/journal.pone.0007301 (2009).
25. Hubel, D. H. & Wiesel, T. N. Receptive fields, binocular interaction and functional architecture in cats visual cortex. *J. Physiol.-London* **160**, 106-& (1962).
26. Devalois, R. L., Albrecht, D. G. & Thorell, L. G. Spatial-frequency selectivity of cells in macaque visual-cortex. *Vision Res.* **22**, 545–559, doi:10.1016/0042-6989(82)90113-4 (1982).

27. Engelage, J. & Bischof, H. J. Single cell responses in the ectostriatum of the zebra finch. *J. Comp. Physiol. A -Neuroethol. Sens. Neural Behav. Physiol.* **179**, 785–795 (1996).
28. Pinto, L. & Baron, J. Spatiotemporal frequency and speed tuning in the owl visual wulst. *Eur. J. Neurosci.* **30**, 1251–1268, doi:10.1111/j.1460-9568.2009.06918.x (2009).
29. Li, D. P., Xiao, Q. & Wang, S. R. Feedforward construction of the receptive field and orientation selectivity of visual neurons in the pigeon. *Cereb. Cortex* **17**, 885–893, doi:10.1093/cercor/bhk043 (2007).
30. Carandini, M. & Heeger, D. J. Normalization as a canonical neural computation. *Nature Reviews Neuroscience* **13**, 51–62, doi:10.1038/nrn3136 (2012).
31. Itti, L. & Koch, C. Computational modelling of visual attention. *Nature Reviews Neuroscience* **2**, 194–203, doi:10.1038/35058500 (2001).
32. Watson, A. B., Barlow, H. B. & Robson, J. G. What does the eye see best? *Nature* **302**, 419–422, doi:10.1038/302419a0 (1983).
33. Kay, K. N., Winawer, J., Rokem, A., Mezer, A. & Wandell, B. A. A Two-Stage Cascade Model of BOLD Responses in Human Visual Cortex. *PLoS Comput. Biol.* **9**, doi:10.1371/journal.pcbi.1003079 (2013).
34. Girshick, A. R., Landy, M. S. & Simoncelli, E. P. Cardinal rules: visual orientation perception reflects knowledge of environmental statistics. *Nat. Neurosci.* **14**, 926-U156, doi:10.1038/nn.2831 (2011).
35. Torralba, A. & Oliva, A. Statistics of natural image categories. *Netw.-Comput. Neural Syst.* **14**, 391–412, doi:10.1088/0954-898x/14/3/302 (2003).
36. Chaparro, A., Stromeyer, C. F., Huang, E. P., Kronauer, R. E. & Eskew, R. T. Color is what the eye sees best. *Nature* **361**, 348–350, doi:10.1038/361348a0 (1993).
37. Guilford, T. The secrets of aposematism - Unlearned responses to specific colors and patterns. *Trends Ecol. Evol.* **5**, 323–323, doi:10.1016/0169-5347(90)90177-f (1990).
38. Wuster, W. *et al.* Do aposematism and Batesian mimicry require bright colours? A test, using European viper markings. *Proceedings of the Royal Society B-Biological Sciences* **271**, 2495–2499, doi:10.1098/rspb.2004.2894 (2004).
39. Sherratt, T. N. & Beatty, C. D. The evolution of warning signals as reliable indicators of prey defense. *American Naturalist* **162**, 377–389, doi:10.1086/378047 (2003).
40. Speed, M. P., Brockhurst, M. A. & Ruxton, G. D. The dual benefits of aposematism: predator avoidance and enhanced resource collection. *Evolution* **64**, 1622–1633, doi:10.1111/j.1558-5646.2009.00931.x (2010).
41. Arbuckle, K., Brockhurst, M. & Speed, M. P. Does chemical defence increase niche space? A phylogenetic comparative analysis of the Musteloidea. *Evol. Ecol.* **27**, 863–881, doi:10.1007/s10682-013-9629-z (2013).
42. Roper, T. J. & Cook, S. E. Responses of chicks to brightly coloured insect prey. *Behaviour* **110**, 276–293, doi:10.1163/156853989x00510 (1989).

43. Roper, T. J. Responses of domestic chicks to artificially coloured insects prey - effects of previous experience and background colour *Anim. Behav.* **39**, 466–473, doi:10.1016/s0003-3472(05)80410-5 (1990).
44. Exnerova, A. *et al.* Importance of colour in the reaction of passerine predators to aposematic prey: experiments with mutants of Pyrrhocoris apterus (*Heteroptera*). *Biological Journal of the Linnean Society* **88**, 143–153, doi:10.1111/j.1095-8312.2006.00611.x (2006).
45. Aronsson, M. & Gamberale-Stille, G. Evidence of signaling benefits to contrasting internal color boundaries in warning coloration. *Behavioral Ecology* **24**, 349–354, doi:10.1093/beheco/ars170 (2013).
46. Kelber, A., Vorobyev, M. & Osorio, D. Animal colour vision - behavioural tests and physiological concepts. *Biological Reviews* **78**, 81–118, doi:10.1017/s1464793102005985 (2003).
47. Osorio, D. & Cuthill, I. C. *Camouflage and Perceptual Organization in the Animal Kingdom*. (Oxford, Oxford University Press, 2015).
48. Endler, J. A. & Basolo, A. L. Sensory ecology, receiver biases and sexual selection. *Trends Ecol. Evol.* **13**, 415–420, doi:10.1016/s0169-5347(98)01471-2 (1998).
49. Ryan, M. J. & Cummings, M. E. Perceptual Biases and Mate Choice. *Annual Review of Ecology, Evolution, and Systematics* **44**, 437-+, doi:10.1146/annurev-ecolsys-110512-135901 (2013).
50. Renoult, J. P. & Mendelson, T. C. Processing bias: extending sensory drive to include efficacy and efficiency in information processing. *Proceedings of the Royal Society B-Biological Sciences* **286**, 10, doi:10.1098/rspb.2019.0165 (2019).
51. Hulse, S. V., Renoult, J. P. & Mendelson, T. C. Sexual signaling pattern correlates with habitat pattern in visually ornamented fishes. *Nat. Commun.* **11**, 8, doi:10.1038/s41467-020-16389-0 (2020).
52. Renoult, J. P., Bovet, J. & Raymond, M. Beauty is in the efficient coding of the beholder. *Royal Society Open Science* **3**, 8, doi:10.1098/rsos.160027 (2016).
53. Haigh, S. M. *et al.* Discomfort and the cortical haemodynamic response to coloured gratings. *Vision Res.* **89**, 47–53, doi:10.1016/j.visres.2013.07.003 (2013).
54. Penacchio, O. & Wilkins, A. J. Visual discomfort and the spatial distribution of Fourier energy. *Vision Res.* **108**, 1–7, doi:10.1016/j.visres.2014.12.013 (2015).
55. Barlow, H. B. *Possible principles underlying the transformations of sensory messages*. (A Symposium. M. I. T. Press, Cambridge 39, Mass., New York, 1961).
56. Osorio, D., Miklosi, A. & Gonda, Z. Visual ecology and perception of coloration patterns by domestic chicks. *Evol. Ecol.* **13**, 673–689, doi:10.1023/a:1011059715610 (1999).
57. Jones, C. D. & Osorio, D. Discrimination of oriented visual textures by poultry chicks. *Vision Res.* **44**, 83–89, doi:10.1016/j.visres.2003.08.014 (2004).
58. Bowmaker, J. K., Heath, L. A., Wilkie, S. E. & Hunt, D. M. Visual pigments and oil droplets from six classes of photoreceptor in the retinas of birds. *Vision Res.* **37**, 2183–2194, doi:10.1016/s0042-6989(97)00026-6 (1997).

59. Osorio, D. & Vorobyev, M. Photoreceptor spectral sensitivities in terrestrial animals: adaptations for luminance and colour vision. *Proceedings of the Royal Society B-Biological Sciences* **272**, 1745–1752, doi:10.1098/rspb.2005.3156 (2005).
60. Serre, T., Oliva, A. & Poggio, T. A feedforward architecture accounts for rapid categorization. *Proc. Natl. Acad. Sci. U. S. A.* **104**, 6424–6429, doi:10.1073/pnas.0700622104 (2007).
61. Palmer, S. E. *Vision Science: Photons to Phenomenology*. (MIT Press, Cambridge, Massachusetts, 1999).
62. CIE. in *Spatial Distribution of Daylight* S 011/E ISO 15469:12003(E) (Commission Internationale de l'Eclairage Standard General Sky, 2003).
63. van Hateren, J. H. & van der Schaaf, A. Independent component filters of natural images compared with simple cells in primary visual cortex. *Proceedings of the Royal Society B-Biological Sciences* **265**, 359–366 (1998).
64. Nascimento, S. M. C., Amano, K. & Foster, D. H. Spatial distributions of local illumination color in natural scenes. *Vision Res.* **120**, 39–44, doi:10.1016/j.visres.2015.07.005 (2016).
65. Team, R. C. R: A Language and Environment for Statistical Computing, R Foundation for Statistical Computing, Vienna, Austria. (2020).
66. Bates, D., Maechler, M., Bolker, B. & Walker, S. lme4: Linear mixed-effects models using Eigen and S4. R package version 1.0–6. http://CRAN.R-project.org/package=lme4. (2014).
67. Matlab, T. M., Inc. MATLAB and Statistics Toolbox Release 2019b, The MathWorks, Inc., Natick, Massachusetts, United States.

Figures

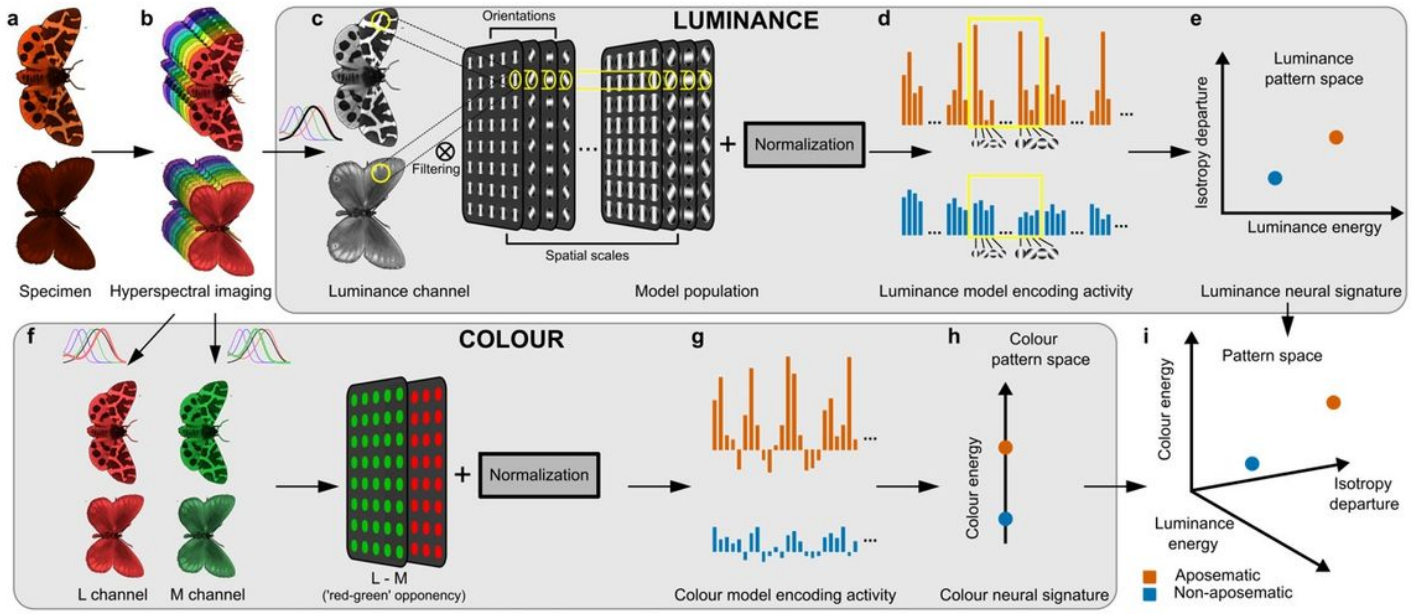

Figure 1

Schematics showing how a perceptual space quantifying patterns was built from a model and image database a, A set of aposematic (top, specimen shown, Arctia caja, dorsum) and non-aposematic species (bottom, Oeneis jutta, dorsum) was identified (referred to as AP and non-AP, respectively). b, Dorsal and ventral sides of specimens were scanned using a hyperspectral imaging system (350-800 nm). c, Modelled luminance pathway. Scans were converted to luminance using the absorption curve of double cones found in chickens (Gallus gallus domesticus). Each black box represents the receptive fields of a population of units regularly distributed on a spatial ('retinotopic') grid and sensitive to edges with a given orientation (4 pictured here) and spatial scale (2 extreme scales represented). The response of the model was computed by considering processing of the luminance images by this population of units, followed by a process of nonlinear normalization of each unit response by the response of neighbouring units. d, Luminance model output. The output of the luminance model was a vector representing activity at each location for each orientation and spatial scale, in response to each pattern. This can be visualised as histograms of activity for each orientation, where each block represents a particular scale. For example, the yellow-boxed region in c delivers higher response at vertical orientation for AP than non-AP patterns (see yellow boxed areas, orange = AP, blue = non-AP). e, Two main summary statistics of the model encoding activity, one based on the strength of the model population response (x-axis, 'luminance energy') and the other one based on the distribution of response strength across orientations (y-axis, 'isotropy departure'), describe a neural signature that can be described as a 'pattern space'. f, Modelled colour pathway. Scans were converted to colour response using cone absorption curves of the chicken. We considered a regularly distributed grid of 'red-green' opponent neurons with a standard normalization. g, The output of the colour model was a vector of encoding activity in response to each pattern (as per d, representing response at each location for each orientation and spatial scale). The AP pattern delivers a more varying response (top) than the non-AP pattern (bottom). h, A one-dimensional colour space was constructed considering a single summary statistic of the colour encoding activity based on the strength of the population response ('colour energy'). i, 3-dimensional luminance and colour neural signatures form a 3-dimensional pattern space in which AP and non-AP patterns occupy distinct locations.

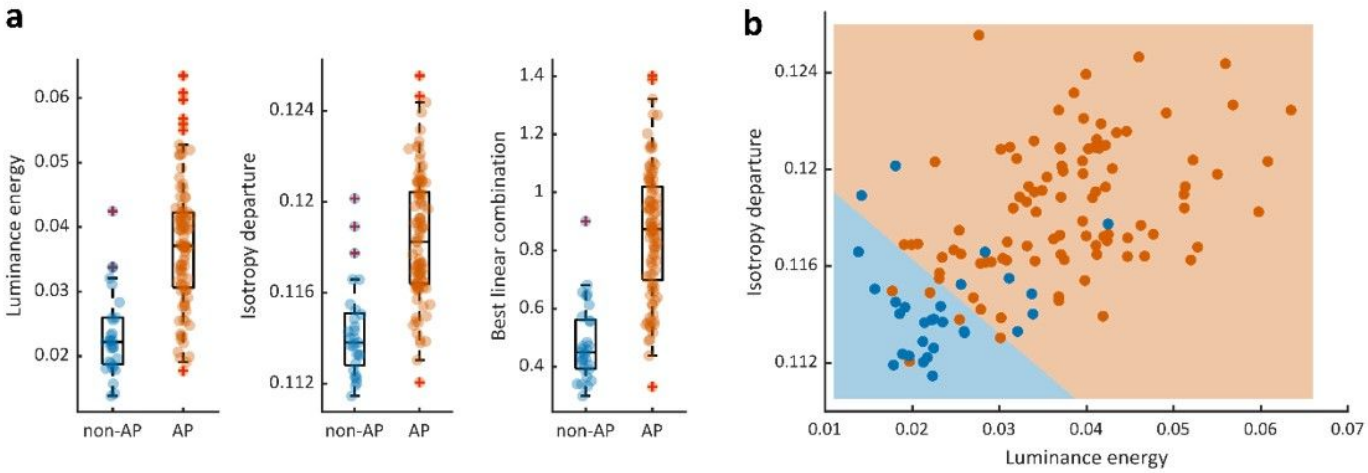

Figure 2

Luminance energy and isotropy departure summary statistics and luminance pattern space. a, Energy, isotropy and the best linear combination between energy and isotropy statistics of the model population activity in response to AP (orange) and non-AP (blue) patterns. Each panel shows the distribution of one of these measures for AP species (orange, N = 96) and non-AP species (blue, N = 29). Each coloured point represents data from a single species, where the statistic value is the average calculated from both sides (dorsal and ventral) of every specimen available for that species. Boxplots show the median, the 25th and 75th percentiles (lower and upper hinges), the lowest measured values within Q1 (first quantile) and 1.5 x Q1 (lower whisker) and the highest observed value within Q3 (third quantile) and 1.5 x Q3 (upper whisker). b, Scatterplot of the energy and isotropy summary statistics defines a 2-dimensional pattern space for the model population activity in response to the Lepidoptera patterns. Each point represents the average over all specimens and sides (dorsal and ventral) for one of the 125 species in the database. The pattern space illustrates an overall higher luminance energy and isotropy departure for the warning signals involved in AP patterns (orange dots) compared to the non-AP species (blue dots). Background colour corresponds to predicted pattern category (pale orange, AP species; pale blue, non-AP) according to the binary classification provided by a logistic regression of pattern category on luminance energy and isotropy departure for the full luminance pattern space (see Methods). Each species can be identified in Supplementary Result 2, Figure S3.

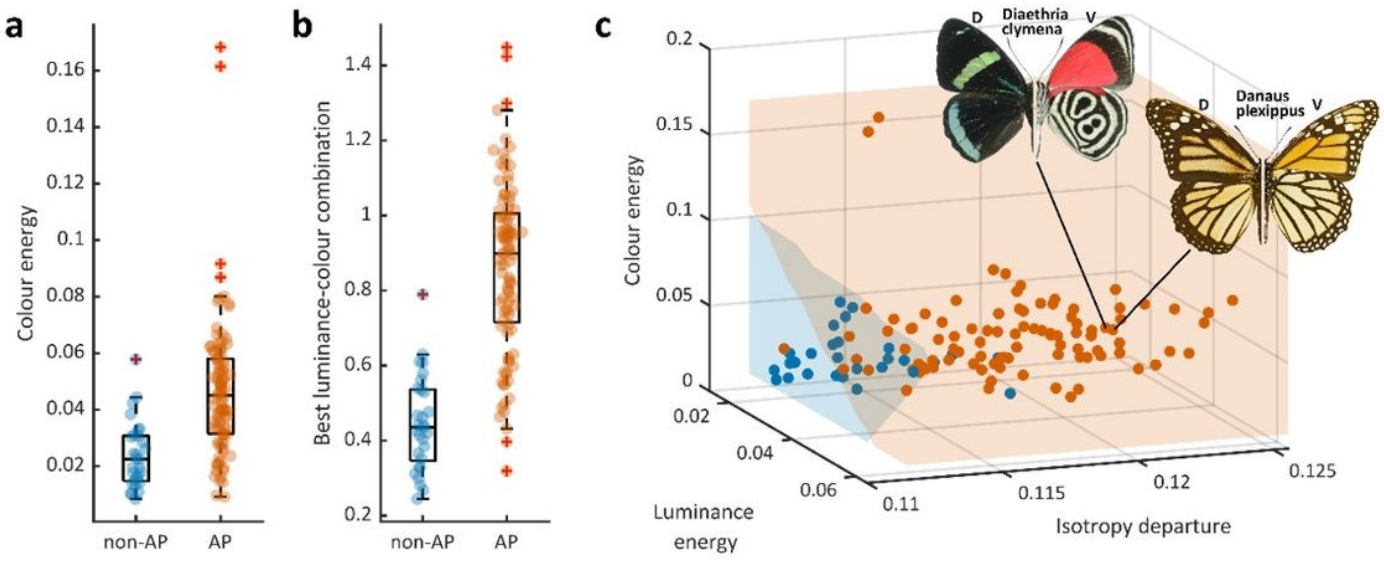

Figure 3

Colour energy neural signature and combined 3-dimensional pattern space. a, Colour energy (left) and b, best linear combination between energy, isotropy departure and colour statistics in response to AP (orange) and non-AP (blue) patterns. Each panel show the distribution of one of these measures for AP species (orange, N = 96) and non-AP species (blue, N = 29). All the conventions are the same as in Fig. 2. c, Scatterplot of the energy, isotropy and colour summary statistics for the model population activity in response to the Lepidoptera patterns. Each dot in this 3-dimensional pattern space represents the average over all specimens and sides (dorsal and ventral) for one of the 125 species in the database. The pattern

space illustrates an overall higher energy, isotropy departure and colour energy for aposematic patterns (orange dots) compared to the patterns of non-aposematic species (blue dots). Background colour corresponds to predicted pattern category (orange, AP species; pale blue, non-AP species) according to the binary classification provided by a logistic regression of pattern category on luminance energy, isotropy departure and colour energy for the full 3-dimensional pattern space. Insets show the dorsal (D, left side) and ventral (V, right side) colouration of two AP species with adjacent neural signatures (Diaethria clymena, left, and Danaus plexippus, right) to illustrate how the patterns of aposematic species can look very different, but have similar statistics. Image credit: D. clymena dorsal and ventral adapted from Geoff Gallice (CC-BY-2.0); D. plexippus adapted from Didier Descouens (CC BY-SA 3.0).

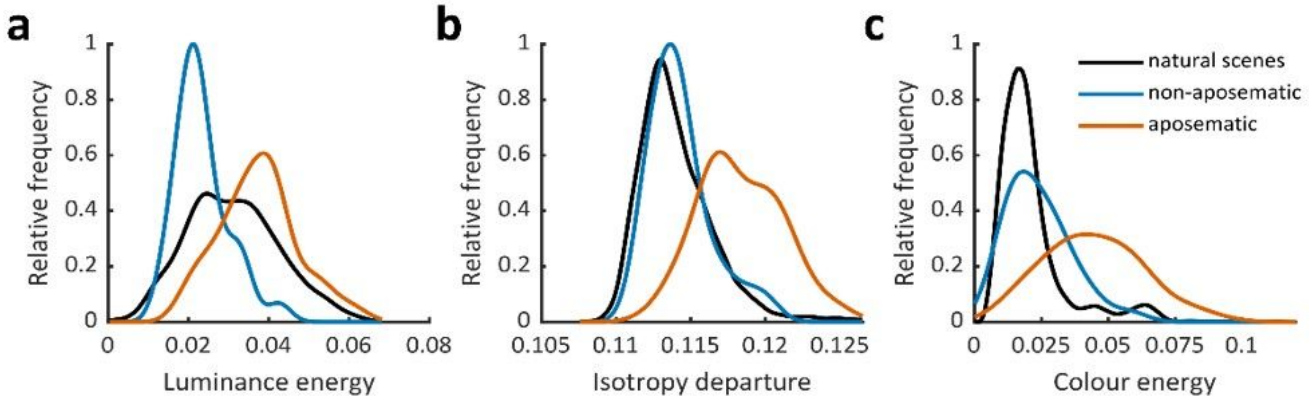

Figure 4

Comparison of neural signatures of aposematic, non-aposematic patterns and natural scenes. Distributions of a, luminance energy, b, isotropy departure and c, colour energy for (black line) natural images, (blue) non-AP species and (orange) AP species. The density plots were obtained using a normal smoothing kernel (see Methods).

Supplementary Files

This is a list of supplementary files associated with this preprint. Click to download.

- TableS1ListofSpecies.xlsx
- TableS2ListofSpecimens.xlsx
- TableS3ListofSupplementarymetrics.xlsx
- SupplementaryMaterialUnderstandingthedesignofwarningsignalsPennacchioetalAugust21.pdf